



The AWAKEN wind farm benchmark, Part 1: Observed conditions

Nicola Bodini¹, Aliza Abraham¹, Paula Doubrawa², Stefano Letizia¹, Julie K. Lundquist^{3,1},
Patrick Moriarty¹, and Ryan Scott⁴

¹National Laboratory of the Rockies, Golden, CO, United States of America

²WSP USA Inc., Boulder, CO, United States of America

³Johns Hopkins University, Baltimore, MD, United States of America

⁴GE Vernova Inc., 58 Charles St, Cambridge, MA 02141, United States of America

Correspondence: Nicola Bodini (nicola.bodini@nlr.gov)

Abstract. Wind turbine wakes significantly reduce downstream performance, yet accurately modeling their sensitivity to atmospheric stability and terrain remains a challenge. To address this, the International Energy Agency Wind Technology Collaboration Programme Task 57 launched a new wind farm wake benchmark leveraging high-resolution observations from the American WAKE experiment (AWAKEN). This paper, Part 1 of a two-part series, details the observational dataset and the selection of 24 August 2023 as the case study for the benchmark. This date was selected for its canonical diurnal cycle, which features a low-level jet with strong nocturnal stratification and high turbulence during the daytime. Analysis of the observational data reveals that despite the relatively simple terrain, interactions between the low-level jet and topography drove significant spatial variability in wind flow, leading to turbine power differences of up to 80 % across the considered wind farm. This paper characterizes these observed conditions to provide a rigorous foundation for the modeling performance evaluation presented in the companion Part 2 paper.

Copyright statement. This work was authored in part by the National Laboratory of the Rockies for the U.S. Department of Energy (DOE), operated under Contract No. DE-AC36-08GO28308. Funding was provided by the U.S. Department of Energy Office of Energy Efficiency and Renewable Energy Wind Energy Technologies Office. The views expressed in the article do not necessarily represent the views of the DOE or the U.S. Government. The U.S. Government retains and the publisher, by accepting the article for publication, acknowledges that the U.S. Government retains a nonexclusive, paid-up, irrevocable, worldwide license to publish or reproduce the published form of this work, or allow others to do so, for U.S. Government purposes.

1 Introduction

Wind turbines extract energy from the atmosphere by slowing down the wind, inevitably creating wakes – regions of reduced wind speed and elevated turbulence – downstream of individual turbines and entire wind plants (Lissaman, 1979). These wakes can extend over several kilometers (Platis et al., 2018; Abraham et al., 2024) and significantly degrade the performance of downstream turbines, reducing overall energy production and increasing structural loads (Thomsen and Sørensen, 1999; Lundquist et al., 2019).



Accurately simulating wind turbine and wind plant wakes remains a complex and open challenge. Wake behavior depends on a wide range of atmospheric and operational conditions, including atmospheric stability (Magnusson and Smedman, 1994; Iungo et al., 2013; Aitken and Lundquist, 2014; Wu et al., 2024), turbulence intensity (Barthelmie et al., 2007), wind veer and shear (Bodini et al., 2017), terrain complexity (Sun et al., 2023; Radünz et al., 2025), surface roughness (Barlas et al., 2016), and turbine operational settings (Modali et al., 2021). Stable atmospheric conditions, in particular, are known to suppress vertical mixing and allow wakes to persist over longer distances (Abkar and Porté-Agel, 2015; Barthelmie et al., 2010) while complex terrain can induce wake deflection and accelerate wake recovery (Castellani et al., 2017; Barthelmie et al., 2018; Wildmann et al., 2018). Furthermore, the coupling between mesoscale atmospheric phenomena (such as low-level jets (LLJs) or convective rolls) and turbine-scale effects is increasingly recognized as a key contributor to wake variability across time and space (Gadde and Stevens, 2021; Quint et al., 2025). As a result, modeling wake-induced losses requires resolving a wide range of scales, which presents a challenge for both stand-alone models and coupled frameworks (Haupt et al., 2023). Trade-offs between computational cost and physical fidelity often determine the choice of modeling approach for a given application, but no consensus yet exists on the most appropriate model type and/or the most appropriate model setup for a given model.

To address these challenges, a wide array of wake modeling approaches has been developed, each with distinct strengths and limitations depending on the target application. At the simplest level, engineering wake models – such as the Jensen/Park (Jensen, 1983; Katic et al., 1987) model – offer fast, analytical solutions based on empirical formulations of wake expansion and momentum conservation. These models are widely used in preliminary layout design and annual energy production estimates and are incorporated into industry software, but often lack the ability to capture background flow and wake dynamics under realistic atmospheric or terrain conditions. More advanced empirical and semi-empirical models, including the dynamic wake meandering model (Larsen et al., 2007, 2013), introduce stochastic components or turbulence-driven dispersion to simulate wake variability and lateral movement. However, these approaches still rely on simplified inflow assumptions and may not accurately reflect interactions between multiple wakes or turbine control strategies (Andersen et al., 2014; Annoni et al., 2014).

Computational fluid dynamics models, particularly those based on Reynolds-averaged Navier-Stokes (RANS) or actuator disk methods, offer greater detail by explicitly solving the governing flow equations around turbine representations (Stergiannis et al., 2016; Letizia and Iungo, 2022; van der Laan et al., 2024). While more computationally expensive, they can simulate wake interactions, shear, and terrain-induced effects with higher resolution. Still, RANS-based approaches often rely on turbulence closure assumptions and may not capture unsteady wake dynamics or mesoscale influences. At the highest (practical) level of fidelity, large-eddy simulations (LES) resolve the largest turbulent eddies in the atmospheric boundary layer and allow for detailed, time-resolved modeling of wake behavior, including wake merging, deflection, and recovery (Jiménez et al., 2010; Wu and Porté-Agel, 2012; Churchfield et al., 2012; Vollmer et al., 2016). LES has proven invaluable in fundamental wake research and control optimization studies, but the computational cost often limits its use to research-grade, short-duration simulations.

Bridging the gap between the levels of fidelity of the options above, the Weather Research and Forecasting (WRF) model (Skamarock et al., 2008) has been increasingly used with embedded wind farm parameterizations to simulate wind energy impacts and wake effects over larger spatial and temporal scales. The WRF model, when coupled with schemes such as the Fitch parameterization or the explicit wake parameterization, incorporates turbine-induced drag and turbulence into the plan-



etary boundary layer physics (Fitch et al., 2012; Volker et al., 2015). These parameterizations treat wind farms as momentum sinks and turbulence sources, enabling the investigation of aggregated wake effects, diurnal variability, and interactions with mesoscale phenomena like LLJs or frontal systems (Arthur et al., 2020; Larsén and Fischereit, 2021; Tomaszewski and Lundquist, 2021). Although WRF-based approaches do not resolve individual turbine wakes explicitly, they are well-suited for capturing farm-scale impacts and can provide valuable inflow conditions for nested LES studies (Vanderwende et al., 2016; Wise et al., 2022).

Despite the broad availability of modeling approaches, comparisons across models and configurations reveal substantial variability in predicted wake effects, even when simulating the same physical scenario (Nygaard et al., 2022). This variability stems not only from differences in model type, but also from user-defined parameters, boundary conditions, and assumptions about turbine operation, atmospheric conditions, and terrain. Moreover, model validation is often carried out using proprietary experimental datasets, which limits replicability and transparency of the results. As a consequence, wake modeling remains a significant source of uncertainty in wind plant performance assessment, long-term energy yield forecasting, and grid integration analyses (Lee and Fields, 2020; Yan et al., 2022). To address this modeling uncertainty and establish a more consistent framework for model evaluation, the International Energy Agency Wind Technology Collaboration Program (IEA Wind) launched Wind Task 57: the Joint Assessment of Wind Energy Models. Task 57 builds on the foundations laid by IEA Wind's previous WakeBench initiative (Task 31, Sanz Rodrigo et al. (2014); Moriarty et al. (2014)), which fostered an international community of researchers, industry partners, and model developers working toward standardized benchmarking of wind and wake models. WakeBench successfully created collaborative benchmarking frameworks, and Task 57 expands these efforts by incorporating new, high-resolution field measurements and advanced uncertainty quantification techniques to critically evaluate and compare state-of-the-art modeling tools.

The first benchmark under Task 57 focuses specifically on wind plant dynamics. Its aim is to systematically assess how well various modeling approaches capture wind conditions and wake features – such as momentum deficits, enhanced turbulence, and the resulting impacts on downstream turbines – under realistic atmospheric and operational conditions. The benchmark design is grounded in data from the American WAKE experimeNt (AWAKEN, Moriarty et al. (2020, 2024)), a large, multi-institutional field campaign designed to provide high-fidelity observations of wind plant–atmosphere interactions. These interactions are a leading source of uncertainty in both preconstruction energy yield assessments and operational forecasting. By offering a robust dataset for model validation, AWAKEN enables more rigorous benchmarking that can ultimately guide improvements in wake modeling tools and reduce uncertainty in wind energy predictions.

This paper presents an overview of AWAKEN and the relevant observations (Sect. 2), the selection of the benchmark case study (Sect. 3) and its observed meteorological and operational conditions (Sect. 4), and conclusions and lessons learned from the planning of the benchmarking exercise (Sect. 5). A companion Part 2 paper (Bodini et al., 2025a) focuses on the modeling results of the benchmark.



90 2 The AWAKEN campaign

The AWAKEN project (Moriarty et al., 2020, 2024) is a large-scale, multi-institutional field campaign designed to observe and simulate interactions between the atmospheric boundary layer and operating wind plants. Running from fall 2022 through summer 2025, AWAKEN focused on a cluster of five wind plants (two of which are shown in Fig. 1) in northern Oklahoma, United States. The campaign is led by the National Laboratory of the Rockies (NLR), with contributions from numerous
95 research institutions primarily funded by the U.S. Department of Energy.

AWAKEN leveraged an extensive and diverse suite of instruments, including lidars (both ground-based and nacelle-mounted), X-band radars, sonic anemometers, thermodynamic profilers, and other meteorological sensors, which are deployed across 13 ground-based sites and five instrumented wind turbines to enable high-resolution characterization of wind plant–atmosphere interactions. Deployment timelines and observations for each instrument platform are available at a2e.energy.gov/project/awaken
100 and in Moriarty et al..

2.1 Wind turbine characteristics

Turbine locations and specifications for the King Plains and Armadillo Flats wind plants were released as part of this benchmark and are available, with the rest of the data released in the benchmark, on Zenodo at <https://doi.org/10.5281/zenodo.15623845> (Bodini et al., 2025b). Table 1 summarizes key parameters for the two wind plants. Due to the proprietary nature of some of
105 the data, the team only received approval to share benchmarking results for the King Plains wind plant, which will be the focus of the results presented here and in the companion paper.

Table 1. Wind plants of interest for the AWAKEN wind plant wake benchmark.

Wind plant	Total rated power	Number of turbines	Turbine model	Rotor diameter	Hub height
King Plains	248.2 MW	88	GE 2.82 MW	127 m	89 m
Armadillo Flats	247.4 MW	23	GE 1.72 MW	103 m	80 m
		57	GE 1.79 MW	100 m	80 m
		46	GE 2.3 MW	116 m	90 m

Open-source turbine models – including thrust and power coefficient curves as well as blade aerodynamic data for each of the four turbine types in Table 1 were provided to the benchmark participants at github.com/NREL/openfast-turbine-models/tree/main/IEA-scaled (NREL, 2025c). Turbine models were created from the IEA 3.4-130 reference turbine through a series of
110 numerical optimizations using the WISDEM/WEIS toolkit (NREL, 2025b). Within WISDEM/WEIS, aeroelastic simulations were run in OpenFAST (NREL, 2025a) with a ROSCO wind turbine controller (NREL, 2021). The structural design process consists of three successive optimizations to produce a target wind turbine from an existing reference: a combined aeroelastic and structural simulation for blade, rotor, and nacelle geometry without stall constraints, a rerun of the preceding step with stall constraints, and a structural simulation for tower geometry. Once the optimized structural model was obtained, turbine

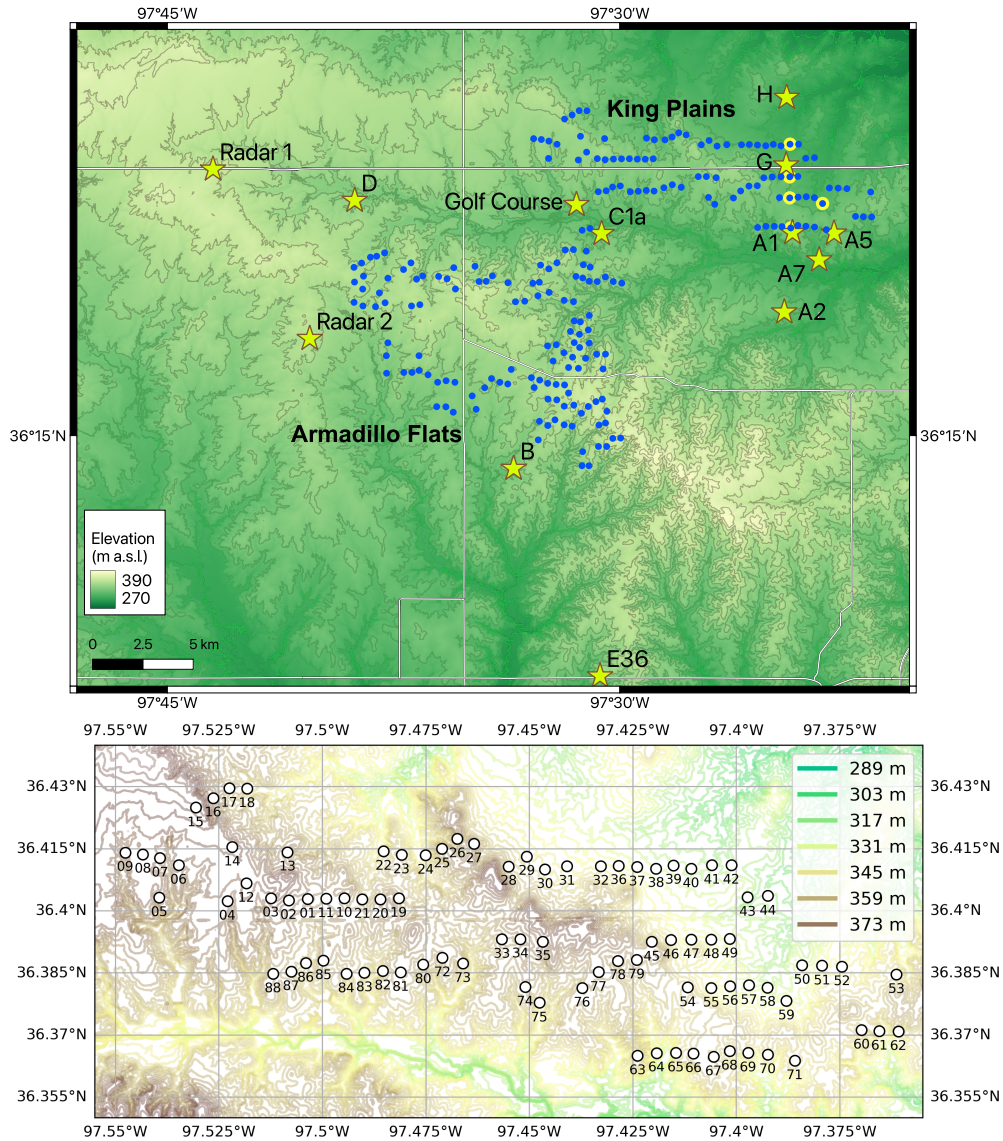


Figure 1. (Top) Map of the King Plains and Armadillo Flats wind plants (blue dots), instrumented sites (yellow stars), and instrumented turbines (yellow dots) in the AWAKEN campaign. The map shows 10 m terrain contours. (Bottom) Identification numbers of the King Plains turbines with terrain contours.

115 performance was evaluated by first tuning the ROSCO controller parameters, then by performing a parameter sweep of wind speeds from 3 to 25 m s⁻¹. Each wind speed was replicated with six random turbulence seeds for a total of 132 simulations per turbine model. Turbine performance was logged in each simulation and averaged across turbulence seeds to produce power and thrust curves. Figure 2 shows the provided open-source power curves of the four turbine types.

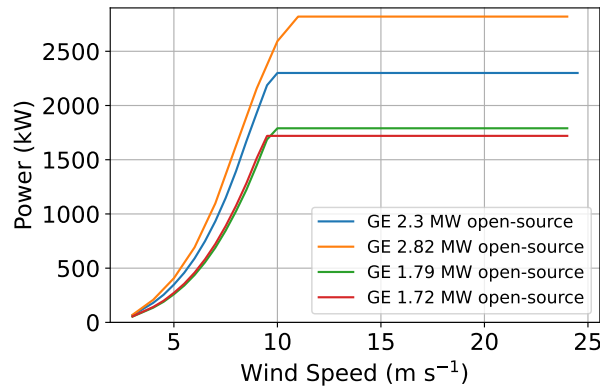


Figure 2. Power curves from the open-source turbine models NLR developed for the wind turbines in the King Plains and Armadillo Flats wind plants.

2.2 Observational network

120 Tables 2 and 3 describe the main instruments that were deployed at the various AWAKEN upwind and downwind sites (assuming dominant winds from the south) and how they operated. Only instruments whose observations were shared as part of the benchmarking activities are included.

In addition to atmospheric observations, supervisory control and data acquisition (SCADA) data from all King Plains turbines are provided (for the 24-hour period corresponding to the benchmark case study). The dataset, at 1-minute resolution, 125 includes turbine-level wind speed (from the nacelle anemometer), wind direction, generated power, yaw misalignment, and a binary flag indicating curtailment. QC was applied to the SCADA data using the OpenOA toolkit (Perr-Sauer et al., 2021) to remove erroneous sensor readings and flag curtailed operation. Normal operation was defined as having a measured wind speed between $[3, 25]$ m s⁻¹ and power between $[1, 102]$ % of rated power output. Periods of curtailment were identified using the relationship between power and blade pitch angle. A turbine generating a certain amount of power was considered curtailed if 130 the blade pitch was more than 10 times the median absolute deviation from the median blade pitch at that power value.

3 Benchmark case study selection

This benchmark centers on a case study designed to evaluate the wind turbine and wind farm wakes within and around the King Plains wind farm (Fig. 1), where the majority of the AWAKEN instrumentation was deployed. The selected case targets wind directions from the south, which are dominant in the region (Krishnamurthy et al., 2021). These conditions allow for the evaluation of both intra-farm wake effects within King Plains and inter-farm wake interactions where Armadillo Flats 135 potentially impacts King Plains.



Table 2. Instrumentation relevant to the benchmark that was deployed at the AWAKEN upwind sites.

Site	Coordinates	Instrumentation	Description
Site A1	36.362° N, 97.405° W	Scanning lidar	Halo Photonics Streamline XR. A 30-minute scan strategy is repeated: 20 minutes of tilted six-beam scans ((Letizia et al., 2024), 20 s each) for vertical profiling, followed by 10 minutes of vertical stare. Data are available from 110 m to 4 km above ground level (a.g.l.) at 10 m intervals. Data are quality-controlled using the dynamic filtering method of Beck and Kühn (2017).
		Profiling lidar	WindCube v2. It profiles horizontal and vertical wind at ~1 Hz resolution, using a five-beam Doppler beam-swinging (DBS) scan. Data are available from 40 m to 240 m a.g.l. in 20 m increments. No systematic quality control (QC) was applied, but carrier-to-noise ratio values are provided.
		Sonic anemometer	Gill R3-50 on a 4 m tripod. It provides 30-minute quality-controlled averages of wind vector, sonic temperature, sensible heat flux, friction velocity, turbulence kinetic energy (TKE), and Obukhov length.
Site A2	36.318° N, 97.409° W	Scanning lidar	Same model and similar scan strategy as Site A1.
		Profiling lidar	WindCube v1. It profiles horizontal and vertical wind at ~1 Hz resolution (published at 2-minute resolution), using a four-beam DBS scan. Data are available from 40 m to 220 m a.g.l. in 20 m increments. Data are quality-controlled with a carrier-to-noise ratio threshold of -22 dB.
		Sonic anemometer	Same as at Site A1.
Site A5	36.362° N, 97.382° W	Sonic anemometer	Same as at Site A1.
Site B	36.232° N, 97.559° W	Profiling lidar	WindCube v2.1. It profiles horizontal and vertical wind at ~1 Hz resolution, using a five-beam DBS scan. Data are available from 40 m to 300 m a.g.l. in 20 m increments. The data are quality-controlled using Vaisala's proprietary filtering algorithm.
		Infrared spectrometer	ASSIST-II, from which temperature and humidity are retrieved via the TROPoe algorithm (Turner and Löhnert, 2021). Data are available as 30-minute profiles from the surface to over 15 km a.g.l., with vertically varying resolution.
Site E36	36.117° N, 97.511° W	Scanning lidar	Halo Streamline XR, deployed in a CLAMPS module. Instantaneous vertical profiles of wind are provided every 10 minutes, from 98.6 m to >10 km a.g.l. in 28 m steps. QC applied using a carrier-to-noise ratio threshold of -23 dB.
		Infrared spectrometer	Same as at Site B, but profiles available at 10-minute resolution.



Table 3. Instrumentation relevant to the benchmark that was deployed at the AWAKEN downwind sites.

Site	Coordinates	Instrumentation	Description
Site C1a	36.362° N, 97.510° W	Profiling lidar	Same as at Site A2.
		Thermodynamic profiler	Same as at Site A1.
Site G	36.399° N, 97.408° W	Thermodynamic profiler	Same as at Site B.
		Sonic anemometer	Same as Site A1.
Golf Course	36.380° N, 97.524° W	Scanning lidar	Same as at Site E36.
		Thermodynamic profiler	Same as at Site E36.
Site H	36.354° N, 97.516° W	Scanning lidar	Same model and similar scan strategy as Site A1.
		Profiling lidar	ZephIR300. The lidar uses a velocity-azimuth display, continuous wave approach. One profile takes about 15–20 s to complete. We provide a vertical profiles of wind at every 20 m from 40 m to 220 m a.g.l..
		Sonic anemometer	Same as at Site A1.
Turbine 41	36.402° N, 97.490° W	Scanning lidar	<p>Halo Streamline XR+ mounted on the nacelle roof. A repeated 2-hour scanning strategy samples both inflow and wake (Letizia et al., 2023):</p> <ul style="list-style-type: none"> – Inflow turbulence scans (00:00–00:30 and every 2 hours after that): Plan position indicator (PPI) scans provide instantaneous radial wind speed over horizontal hub-height plane. – Wake meandering scans (00:30–01:00 and every 2 hours after that): PPI and range height indicator scans provide instantaneous radial wind speed over horizontal hub-height plane and over vertical plane aligned with turbine yaw position. – Inflow statistics scans (01:00–01:20 and every 2 hours after that): PPI scans provide 20-minute average streamwise incoming wind speed and yaw misalignment at hub height. – Wake 3D statistics scans (01:00–01:40 and every 2 hours after that): Volumetric scans provide 20-minute average streamwise wind speed and its standard deviation at 3D locations in the turbine wake. – Farm statistics scans (01:40–02:00 and every 2 hours after that): Volumetric scans provide 20-minute average streamwise wind speed and its standard deviation at 3D locations in the farm wake.



Given the extensive duration of the AWAKEN field campaign and the large volume of data collected, an automated search algorithm was developed to identify a one-day reference case that satisfies specific observational and operational criteria. In particular, we focus on periods when: (i) more than 80 % of turbines in both the King Plains and Armadillo Flats wind farms were operating normally the whole day; (ii) nacelle-mounted lidar data from the northernmost instrumented turbine in King Plains (Turbine 41) were available; (iii) ground-based lidar data from sites A1 and H were available; and (iv) the wind direction at 90 m (measured at Site A1) ranged between 135° and 225° (dominant conditions). Approximately 700 hours of observations meet all these conditions. However, only a few days maintain them consistently over a full diurnal cycle, which is essential for capturing the temporal variability in wake behavior.

Based on these constraints, we selected 24 August 2023 as the benchmark case study. In addition to meeting all predefined criteria, this day exhibits canonical thermodynamic profiles, with no adverse synoptic conditions (e.g., frontal passages, precipitation), and with consistent turbine availability throughout the day. Benchmark participants were tasked with simulating conditions around the King Plains (and Armadillo Flats) wind farms on this date. Participants determined their own simulated spatial extents, though we strongly recommended including both wind farms to capture inter-farm wake dynamics.

4 Observed conditions on 24 August 2023

Observed wind conditions on 24 August 2023 are shown in Fig. 3 (the thermodynamic observations discussed in (Bodini et al., 2024) show no clouds or precipitation). A typical diurnal cycle is apparent, with low shear and enhanced turbulence during the local afternoon and a stable boundary layer overnight. A double LLJ is observed. The second LLJ, occurring between 10 UTC and 15 UTC, is located higher in the atmosphere and is unlikely to significantly affect turbine operation with its core features. In contrast, the first LLJ, from 4 UTC to 9 UTC, has a much lower jet nose that partially intersects turbine hub heights, posing a greater potential impact on power production. Comparing observations at the three lidar sites (A1, A2, and H), we find considerable spatial variability in the LLJ structure (Rai et al., 2026). The first LLJ is lowest at Site A2 (upwind and far from the turbines), slightly higher at Site A1 (upwind but adjacent to the southernmost King Plains turbines), and highest at Site H (downwind of the King Plains wind farm).

To examine this LLJ-related variability more closely, Fig. 4 shows time series of the LLJ nose height, hub-height (for the King Plains turbines) wind speed and direction, rotor-averaged lidar-derived turbulence kinetic energy (TKE), and shear exponent and wind veer across the turbine rotor layer from lidars at A1, A2, and H. The first LLJ develops a nose between 140 and 300 m above ground level, indicating strong interaction with the turbine rotor layer. While the LLJ initially has a similar structure across sites around 3–4 UTC, site-specific differences develop between 5 and 7 UTC. During this period, the LLJ nose is lowest at A2, with a vertical difference of roughly 100 m compared to Site H. Consequently, hub-height wind speed peaks at A2 and is substantially lower at A1 and H, i.e., over the King Plains wind plant, while wind direction remains relatively constant across all sites.

The cause of this localized lifting of the LLJ remains uncertain, though terrain-driven processes are a likely factor. Notably, TKE peaks sharply at Site H (and to a lesser extent at Site A1) around 6 UTC. While Site H typically exhibits elevated TKE

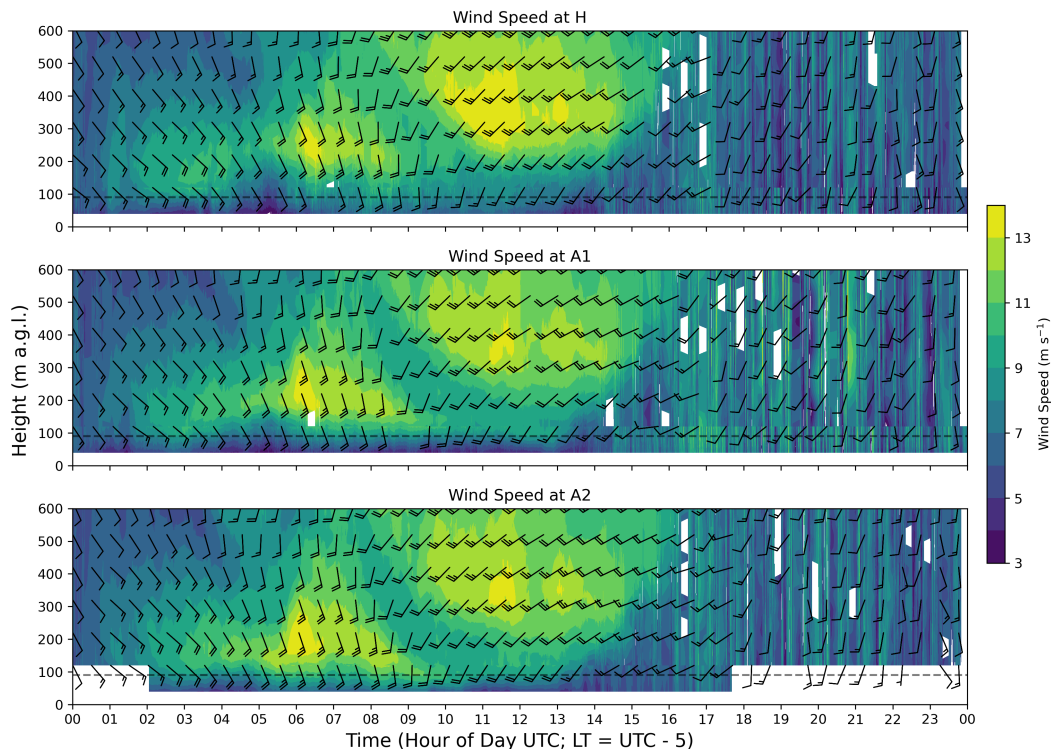


Figure 3. Time–height cross section of observed wind speed with wind barbs to show wind direction across the AWAKEN domain on 24 August 2023 as observed from the lidars at sites A1 (middle), A2 (bottom), and H (top). Data from profiling lidars are shown through 120 m a.g.l., while data from the scanning lidars are used for higher altitudes. The horizontal dashed line indicates hub height for the King Plains turbines.

170 due to wake effects, the pronounced peak could indicate a hydraulic jump forming in the valley between A2 and A1, similar to what Peña and Santos (2021) found. The lack of a corresponding sharp TKE increase at A1 suggests that such a jump might be localized near the slope or that A1 is situated just upstream of the turbulent break-point of the wave. Alternatively, as detailed by Zhou and Chow (2014) for similar terrain in the CASES-99 experiment, near-surface terrain-induced turbulence—specifically gravity wave breaking over valley cold-air pools—can trigger shear instabilities that effectively displace

175 the stable layer upward, causing the LLJ nose to ride above the turbulent zone. Also, the proximity of the King Plains wind plant suggests that the plant itself may be contributing to the flow deformation. As observed by Krishnamurthy et al. (2025); Rai et al. (2026), the cumulative wake of a large wind plant can lead to a “deep array effect”, where the flow is forced upward over the plant, potentially lifting the LLJ nose height for downstream or interior sites.

Regardless of the precise mechanism – be it terrain-induced, wake-induced, or a combination of both – these observations

180 demonstrate that initializing a numerical model with wind speed data from Site A2 only would lead to a large overestimation



of power generation for the King Plains wind plant. Despite the relatively simple terrain in this region, significant wind speed differences arise from local interactions between the LLJ, topography, and the wind turbines themselves.

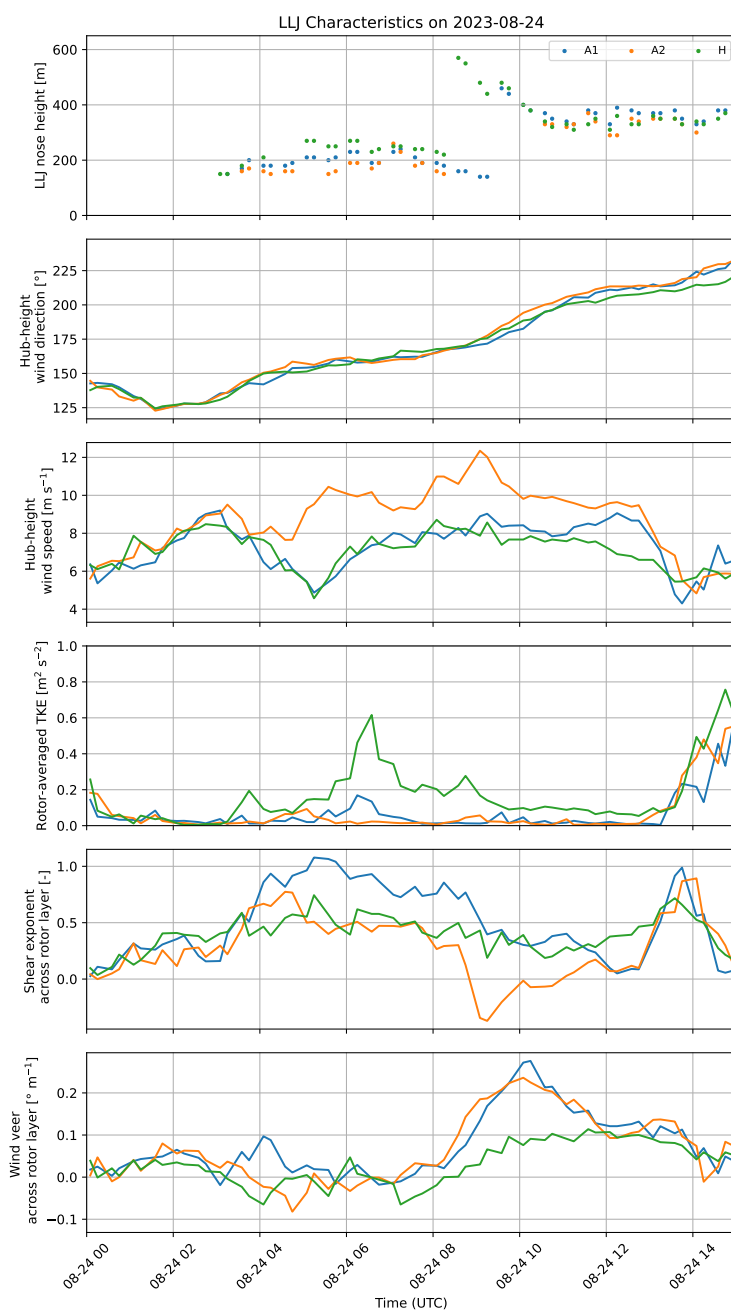


Figure 4. Time series of LLJ nose height, hub-height wind direction, hub-height wind speed, rotor-averaged lidar TKE, shear exponent across the turbine rotor layer, and wind veer across the turbine rotor layer at sites A1, A2, and H.



185 These spatial and temporal variations in wind conditions translate directly into variability in turbine power production, as recorded by the King Plains SCADA system. Most turbines from both wind plants were operating normally on 24 August 2023, with no significant drop in availability outside of some high-frequency fluctuations. However, Fig. 5 reveals substantial temporal variability in turbine-level power, particularly during stable nighttime conditions. A pronounced drop in power occurs around 5:30 UTC, coinciding with the local lifting of the LLJ identified in Figs. 3 and 4. Spatial heterogeneity is also evident: Turbines in different locations across the farm exhibit power output differences of up to 80 % at a given time during the night (e.g., around 9 UTC).

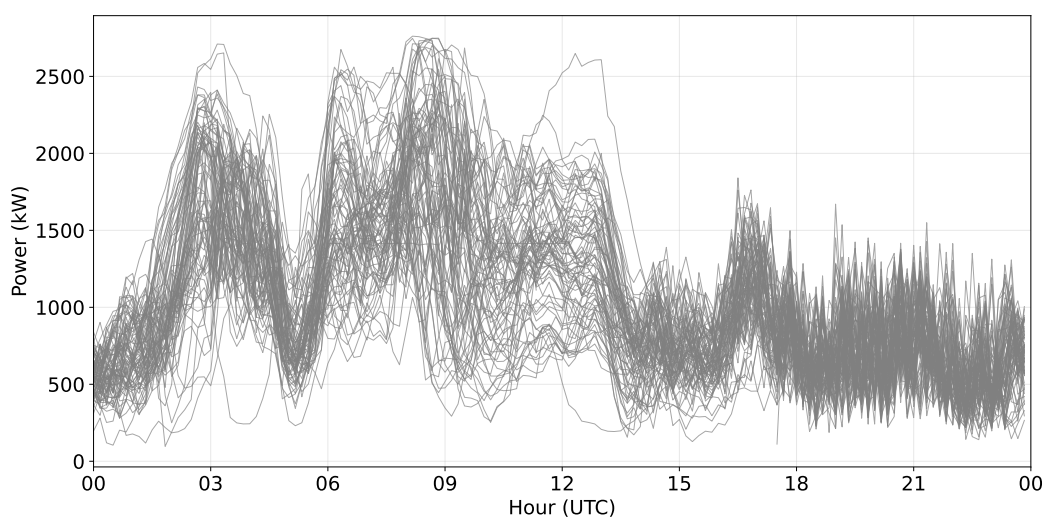


Figure 5. Time series showing the power production by each King Plains turbine on 24 August 2023.

190 The spatial variability in power production can be further explored by looking at a map of total energy production by each King Plains turbine on the benchmark day (Fig. 6). Turbines in the northern and eastern portions of the farm produce more energy overall. The east-west gradient may be expected given the prevailing south-southwesterly winds and potential farm-to-farm wake effects from the upwind Armadillo Flats wind farm. However, the north-south gradient is less intuitive: Northern turbines, which should be more impacted by internal wakes, still produce more energy, perhaps similar to the case study of
195 Radünz et al. (2025). Interestingly, Turbine 53 in the eastern portion of the wind plant shows the highest energy output, likely due to local terrain-induced speedups.

The main patterns of spatial variability in energy production are systematically assessed by computing empirical orthogonal functions (EOFs) of turbine-level energy production across the King Plains wind farm for the benchmark day (Fig. 7 top). We note that while EOF signs are arbitrary, the relative phase differences between turbines are preserved to maintain physical
200 interpretability. The first mode appears to capture coherent, farm-wide fluctuations in production that likely reflect changes in the large-scale wind speed, excluding turbines that were offline or significantly curtailed (which appear as a zero EOF loading). The second mode we attribute to the combined influence of external wakes and topography: turbines in the western portion of

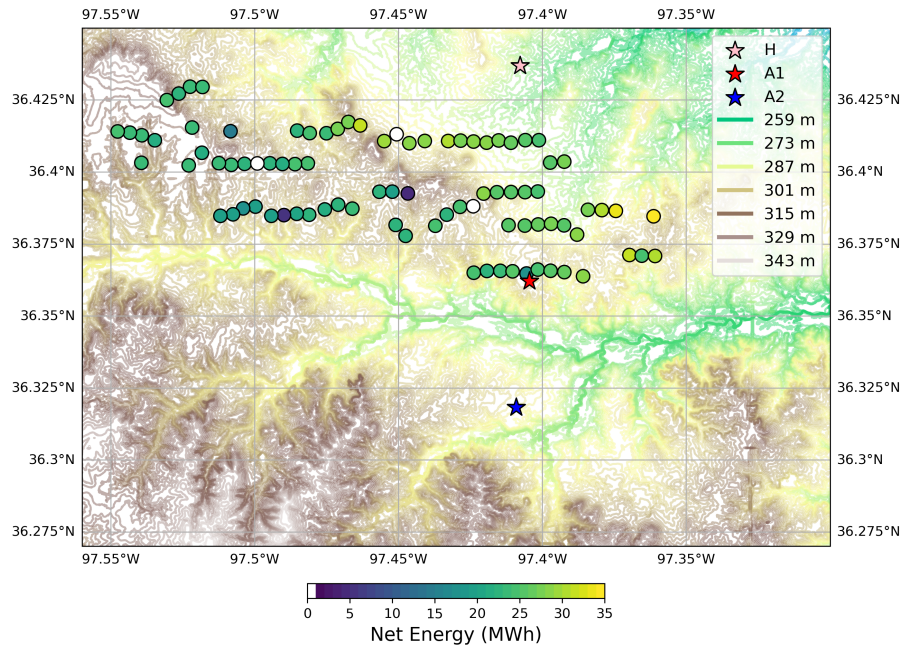


Figure 6. Map of the total energy production by the King Plains turbines on 24 August 2023.

King Plains exhibit reduced production consistent with wake impacts from Armadillo Flats, while turbines in the eastern sector show enhanced production likely associated with terrain-induced speedups. The third mode seems to isolate patterns of internal
 205 wake variability, with consistently lower production in downstream turbines—especially within East King Plains, which is not directly affected by Armadillo Flats. Together, however, the first three modes explain less than 65 % of the total variance (Fig. 7 bottom), highlighting the substantial complexity and heterogeneity of turbine-level power production on a daily scale.

To further confirm how terrain influences the spatial variability of power production, we calculated a relative elevation metric for each turbine. For every stability class (determined using the Obukhov length calculated from sonic anemometer
 210 measurements collected at Site A1), we defined an upstream sector centered on the mean hub-height wind direction (from the profiling lidar at Site A1). This sector was defined by a 1 km radius and a 45° arc. We then calculated the mean terrain elevation within this upstream sector ($\bar{z}_{upstream}$) and subtracted it from the specific turbine’s base elevation ($z_{turbine}$):

$$\Delta z_{rel} = z_{turbine} - \bar{z}_{upstream} \quad (1)$$

This Δz_{rel} value represents the turbine’s elevation relative to the terrain it “sees” immediately upwind. A positive value
 215 indicates the turbine is situated higher than the upstream fetch (e.g., a ridge, hilltop, or positive slope) relative to the incoming flow, while a negative value indicates a local depression or negative slope. By calculating this for each stability class, we account for the fact that the “effective” upwind terrain changes as the mean wind direction shifts with atmospheric stability. Figure 8 shows turbine power output as a function of this upwind elevation difference for stable and unstable conditions. In both cases, turbines situated lower than the upwind terrain (left side of the plots) tend to produce more power, especially

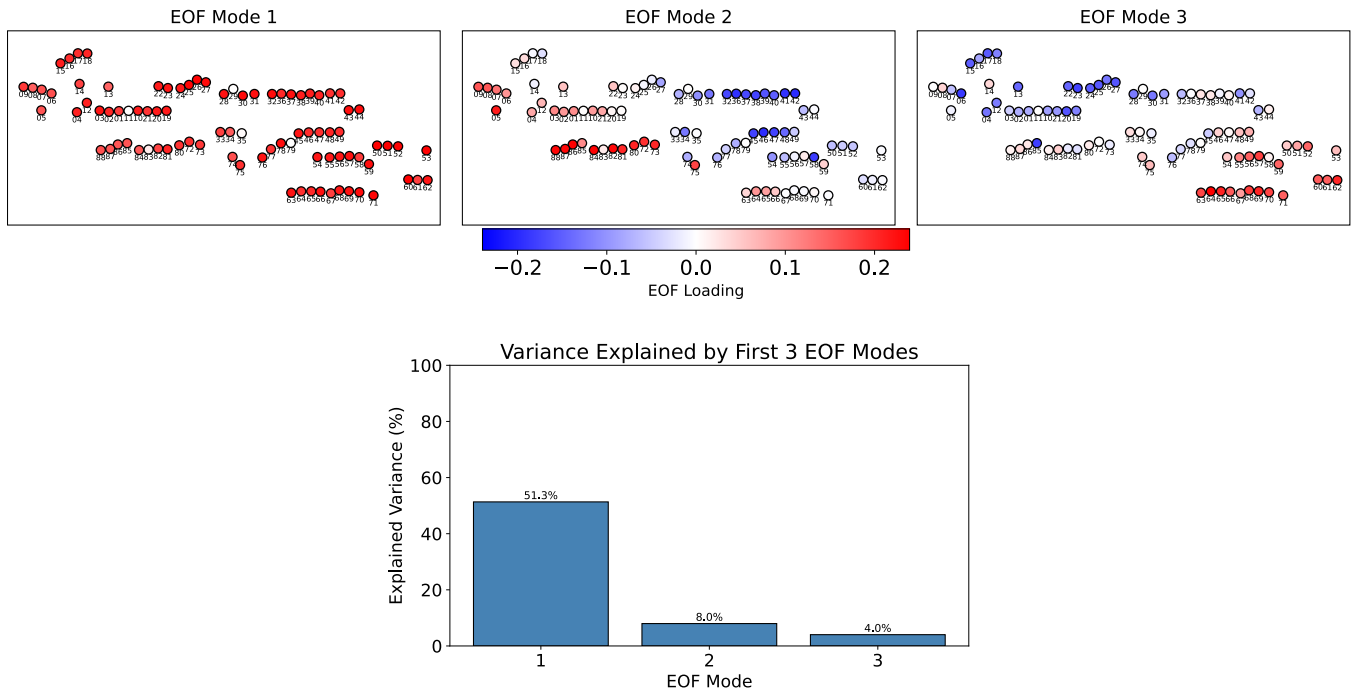


Figure 7. (Top) Spatial variability in energy production by King Plains turbines expressed by the first three EOF modes. (Bottom) Variance explained by the first three EOF modes.

220 under stable conditions, despite being located downwind of other turbines in the King Plains case. This counterintuitive result aligns with numerical findings from Radünz et al. (2025), who suggested that terrain-induced acceleration of hub-height winds can outweigh the effects of turbine wakes at the AWAKEN site, particularly under stably stratified conditions. These results suggest that models relying solely on flat-terrain assumptions or standard wake decay curves without terrain corrections will likely misinterpret the performance drivers on this day.

225 During the selected case study, most turbines were operating in Region 2 of their power curve, when thrust coefficient is high and wakes are the strongest. Total curtailment, shown in Fig. 9, was defined as the proportion of curtailed time stamps relative to normal operating time stamps for the benchmark day. King Plains turbines 11, 29, and 79 (see locations in Fig. 1) were off for the entire benchmark day.

230 While terrain-related effects might make wake signatures murkier, the comprehensive AWAKEN measurements still allow for their assessment and characterization. As detailed in Bodini et al. (2024), the suite of scanning and profiling lidars – deployed on the ground, on turbine nacelles, and on a mobile platform – captured the wind plant wake dynamics at King Plains during the selected case study. A clear wake-induced wind speed deficit of over 1 m s^{-1} was observed at Site H, located 22 rotor diameters downwind of King Plains, particularly above the turbine hub height (Fig. 10). These wake impacts were most evident during nighttime stable conditions when low turbulent mixing delayed wake recovery and the LLJ was lifted.

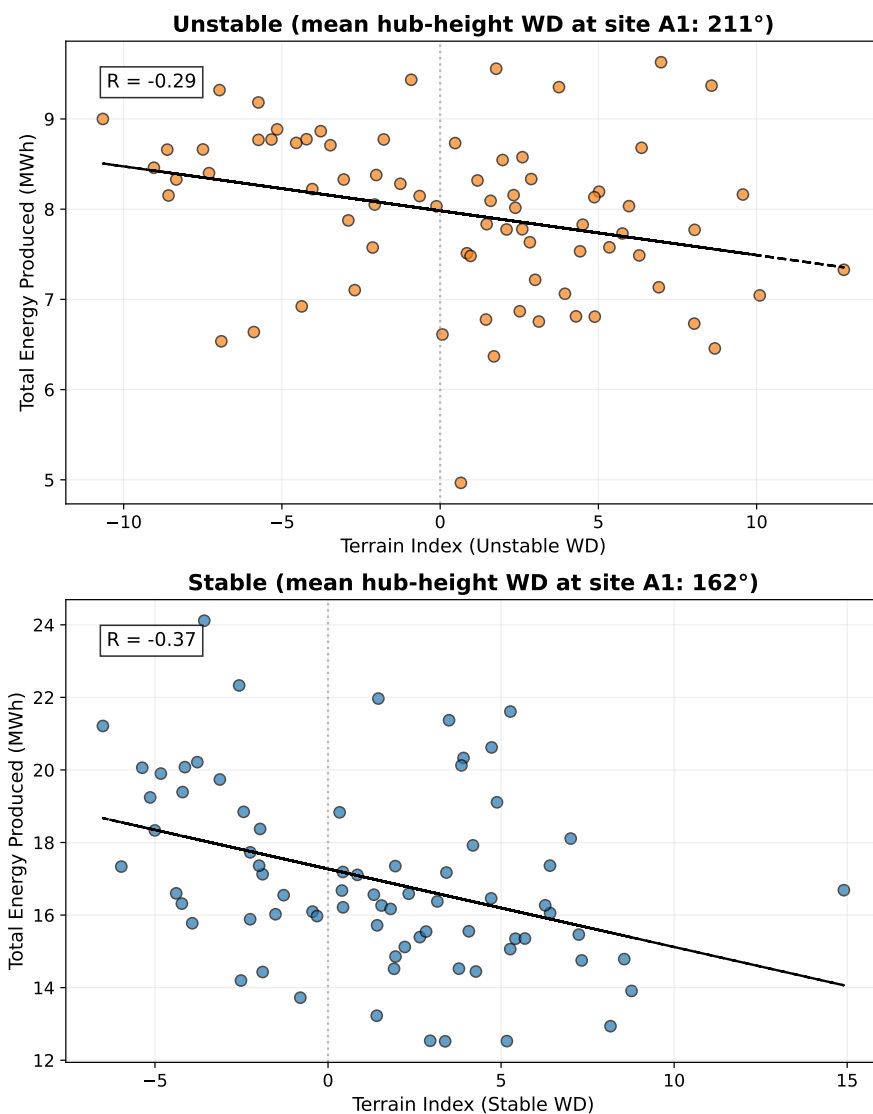


Figure 8. Total energy produced by King Plains turbines as a function of upwind (45° sector aligned with the mean hub-height wind direction (WD) measured at Site A1 for each stability class) terrain variability, for (top) stable and (bottom) unstable conditions on 24 August 2023. Turbines that experienced curtailment are not included.

235 In contrast, under daytime unstable conditions, enhanced turbulence eroded the wakes almost entirely before reaching Site H. Additionally, nacelle-mounted lidars on the northernmost row of King Plains turbines revealed the spatiotemporal evolution of single-turbine wake structures and their dependence on atmospheric stability.

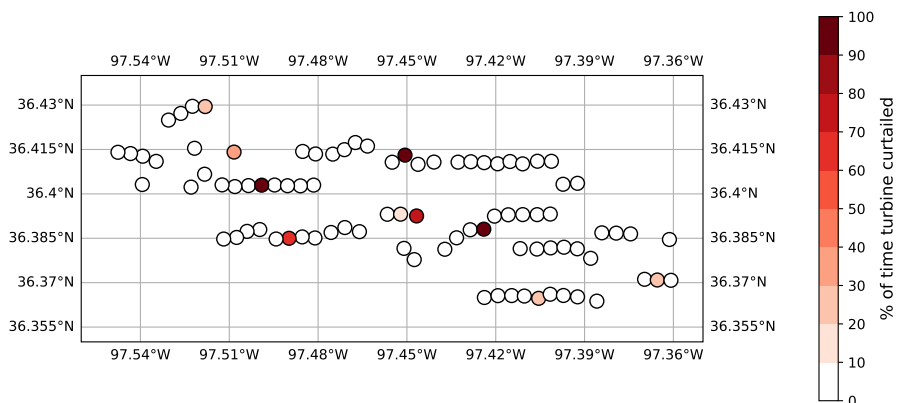


Figure 9. Map showing the percentage of time each turbine at the King Plains wind farm experienced curtailment during the benchmark day.

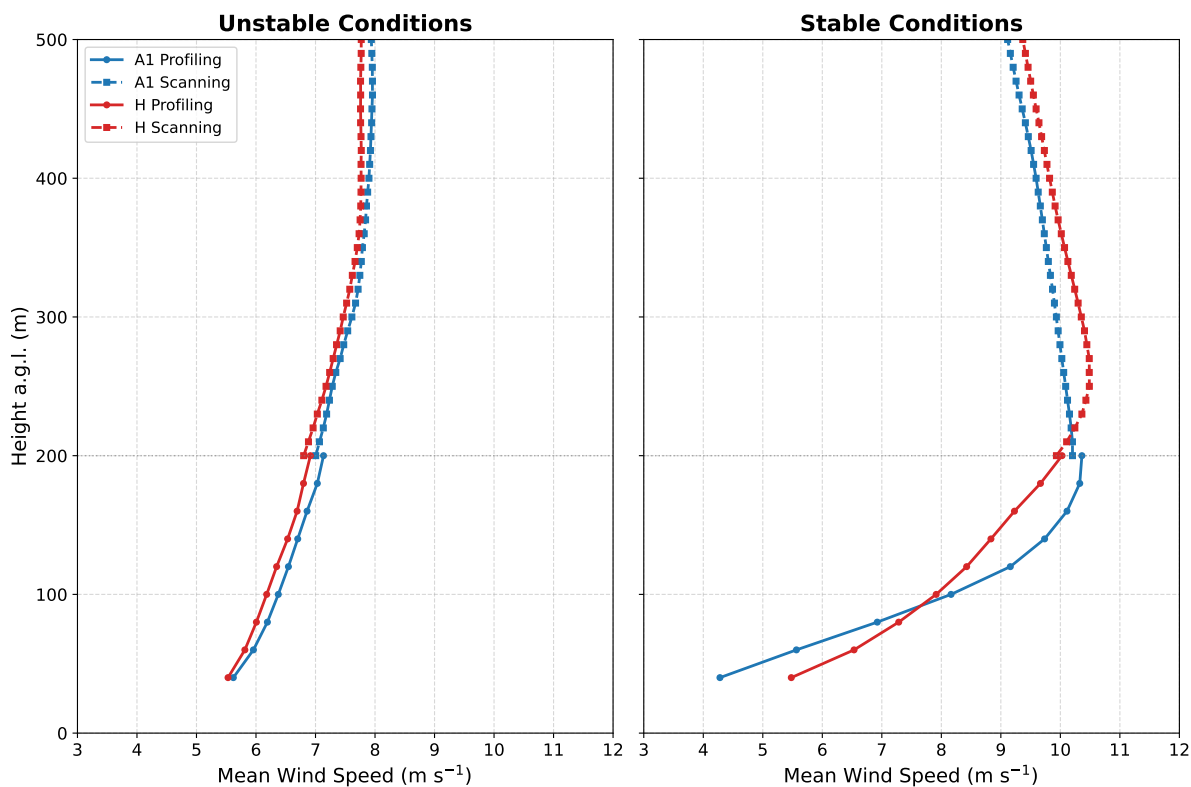


Figure 10. Mean vertical profiles of wind speed at sites A1 (blue) and H (red) during unstable (left) and stable (right) atmospheric conditions on the benchmark day. Profiles are constructed using a composite of profiling lidar data for the rotor layer ($z \leq 200$ m; solid lines) and scanning lidar data for the upper boundary layer ($z \geq 200$ m; dashed lines); hence the discontinuity at 200 m.



5 Conclusions

This paper introduces the design and observational foundation of the IEA Wind Task 57 wind plant wake benchmark. Leveraging the unprecedented multi-platform measurements from the AWAKEN campaign, the benchmark provides a rigorously curated case study – 24 August 2023 – selected through an automated search process to ensure high data availability, consistent turbine operations, and meteorological representativeness.

The analysis of the selected case study highlights the critical importance of resolving wind flow features across scales. Observations on 24 August 2023 revealed that a single vertical profile is insufficient to characterize inflow even in moderately complex terrain. We observed a localized lifting of the LLJ nose by approximately 100 m between sites across the AWAKEN domain, which correlated with significant power drops. Furthermore, a counterintuitive correlation between lower terrain elevation and higher power output was observed under stable conditions, suggesting terrain-induced speedups outweigh wake losses in specific stability regimes.

With the development of this benchmark, the goal was to create a controlled, transparent, and scientifically valuable framework that enables the wind energy modeling community to evaluate and improve wake modeling approaches. Several key lessons emerged from the process of organizing this benchmark. Sufficient time must be allocated for data QC and analysis before launching a benchmark, as these are critical to building trust in the dataset used to validate numerical models. Moreover, as is typical in large, multi-instrument field campaigns, full and simultaneous data availability across all platforms cannot be guaranteed. Recognizing these practical limitations is essential, and thoughtful compromises are often required. The modeling results and analysis from all three phases of the benchmark are presented in the companion Part 2 journal article.

Data availability. The AWAKEN data released as part of this benchmark are available on Zenodo at <https://doi.org/10.5281/zenodo.15623845> (Bodini et al., 2025b). Publicly available AWAKEN observations are available at <https://doi.org/10.21947/AWAKEN/1914202> (Wind Data Hub, 2022).

Author contributions. NB: Conceptualization, Methodology, Formal analysis, Investigation, Validation, Writing - Original Draft. AA, SL, RS: Data Curation, Writing - Review & Editing. JKL: Conceptualization, Writing - Review & Editing. PM: Conceptualization, Funding acquisition, Writing - Review & Editing.

Competing interests. At least one of the (co-)authors is a member of the editorial board of *Wind Energy Science*. The authors have no other competing interests to declare.

<https://doi.org/10.5194/wes-2026-33>
Preprint. Discussion started: 23 February 2026
© Author(s) 2026. CC BY 4.0 License.



Acknowledgements. The authors would like to thank ENGIE and GE for agreeing to release proprietary data for the King Plains wind farm
265 to enable the execution of the benchmark.



References

- Abkar, M. and Porté-Agel, F.: Influence of atmospheric stability on wind-turbine wakes: A large-eddy simulation study, *Physics of fluids*, 27, <https://doi.org/10.1063/1.4913695>, 2015.
- Abraham, A., Hamilton, N., Bodini, N., Hirth, B., Schroeder, J., Letizia, S., Krishnamurthy, R., Newsom, R., and Moriarty, P.: Land-based
270 wind plant wake characterization using dual-Doppler radar measurements at AWAKEN, *Journal of Physics: Conference Series*, 2767, 092 037, <https://doi.org/10.1088/1742-6596/2767/9/092037>, 2024.
- Aitken, M. L. and Lundquist, J. K.: Utility-scale wind turbine wake characterization using nacelle-based long-range scanning lidar, *Journal of Atmospheric and Oceanic Technology*, 31, 1529–1539, <https://doi.org/10.1175/JTECH-D-13-00218.1>, 2014.
- Andersen, S. J., Sørensen, J. N., Ivanell, S., and Mikkelsen, R. F.: Comparison of engineering wake models with CFD simulations, *Journal of physics: Conference series*, 524, 012 161, <https://doi.org/10.1088/1742-6596/524/1/012161>, 2014.
- 275 Annoni, J., Seiler, P., Johnson, K., Fleming, P., and Gebraad, P.: Evaluating wake models for wind farm control, in: 2014 American Control Conference, pp. 2517–2523, IEEE, <https://doi.org/10.1109/ACC.2014.6858970>, 2014.
- Arthur, R. S., Mirocha, J. D., Marjanovic, N., Hirth, B. D., Schroeder, J. L., Wharton, S., and Chow, F. K.: Multi-scale simulation of wind farm performance during a frontal passage, *Atmosphere*, 11, 245, <https://doi.org/10.3390/atmos11030245>, 2020.
- 280 Barlas, E., Buckingham, S., and van Beeck, J.: Roughness effects on wind-turbine wake dynamics in a boundary-layer wind tunnel, *Boundary-Layer Meteorology*, 158, 27–42, <https://doi.org/10.1007/s10546-015-0083-z>, 2016.
- Barthelmie, R., Pryor, S., Wildmann, N., and Menke, R.: Wind turbine wake characterization in complex terrain via integrated Doppler lidar data from the Perdigão experiment, *Journal of Physics: Conference Series*, 1037, 052 022, <https://doi.org/10.1088/1742-6596/1037/5/052022>, 2018.
- 285 Barthelmie, R. J., Frandsen, S. T., Nielsen, M., Pryor, S., Rethore, P.-E., and Jørgensen, H. E.: Modelling and measurements of power losses and turbulence intensity in wind turbine wakes at Middelgrunden offshore wind farm, *Wind Energy: An International Journal for Progress and Applications in Wind Power Conversion Technology*, 10, 517–528, <https://doi.org/10.1002/we.238>, 2007.
- Barthelmie, R. J., Pryor, S. C., Frandsen, S. T., Hansen, K. S., Schepers, J., Rados, K., Schlez, W., Neubert, A., Jensen, L., and Neckelmann, S.: Quantifying the impact of wind turbine wakes on power output at offshore wind farms, *Journal of Atmospheric and Oceanic
290 Technology*, 27, 1302–1317, <https://doi.org/10.1175/2010JTECHA1398.1>, 2010.
- Beck, H. and Kühn, M.: Dynamic data filtering of long-range Doppler LiDAR wind speed measurements, *Remote sensing*, 9, 561, <https://doi.org/10.3390/rs9060561>, 2017.
- Bodini, N., Zardi, D., and Lundquist, J. K.: Three-dimensional structure of wind turbine wakes as measured by scanning lidar, *Atmospheric Measurement Techniques*, 10, 2881–2896, <https://doi.org/10.5194/amt-10-2881-2017>, 2017.
- 295 Bodini, N., Abraham, A., Doubrawa, P., Letizia, S., Thedin, R., Agarwal, N., Carmo, B., Cheung, L., Radünz Corrêa, W., Gupta, A., Gupta, A., Goldberger, L., Hamilton, N., Herges, T., Hirth, B., Iungo, G. V., Jordan, A., Kaul, C., Klein, P., Krishnamurthy, R., Lundquist, J. K., Maric, E., Moriarty, P., Moss, C., Newsom, R., Pichugina, Y., Puccioni, M., Quon, E., Roy, S., Rosencrans, D., Sanchez Gomez, M., Scott, R., Shams Solari, M., Taylor, T. J., and Wharton, S.: An international benchmark for wind plant wakes from the American WAKE Experiment (AWAKEN), *Journal of Physics: Conference Series*, 2767, 092 034, <https://doi.org/10.1088/1742-6596/2767/9/092034>, 2024.
- 300 Bodini, N., Abraham, A., Doubrawa, P., Letizia, S., Lundquist, J. K., Moriarty, P., Scott, R., Thedin, R., Archer, C., Blaylock, M., Bottasso, C., Braunbehrens, R., Carmo, B., Cheung, L., Dubreuil, C., Floors, R., Herges, T., Houck, D., Kanhari, A., Kaul, C., Kelley, C., Li, R., Major, D., Nguyen, A. K., Optis, M., Parada, L., Peña, A., Quick, J., Radünz, W., Rai, R., Santiago, O. M. G., Schulte, J., van der Laan,



- P., Vimalakanthan, K., and Wise, A.: The AWAKEN wind farm modeling benchmark. Part 2: benchmark results, *Wind Energy Science*, in review, 2025a.
- 305 Bodini, N., Abraham, A., Letizia, S., Scott, R., Moriarty, P., and Thedin, R.: AWAKEN wind farm wake benchmark inputs, <https://doi.org/10.5281/zenodo.15623845>, data released as part of the IEA Wind Task 57 JAM benchmark activities, covering all three phases of the exercise. Case study date: 24 August 2023., 2025b.
- Castellani, F., Astolfi, D., Mana, M., Piccioni, E., Becchetti, M., and Terzi, L.: Investigation of terrain and wake effects on the performance of wind farms in complex terrain using numerical and experimental data, *Wind Energy*, 20, 1277–1289, <https://doi.org/10.1002/we.2094>,
310 2017.
- Churchfield, M. J., Lee, S., Michalakes, J., and Moriarty, P. J.: A numerical study of the effects of atmospheric and wake turbulence on wind turbine dynamics, *Journal of turbulence*, p. N14, <https://doi.org/10.1080/14685248.2012.668191>, 2012.
- Fitch, A. C., Olson, J. B., Lundquist, J. K., Dudhia, J., Gupta, A. K., Michalakes, J., and Barstad, I.: Local and mesoscale impacts of wind farms as parameterized in a mesoscale NWP model, *Monthly Weather Review*, 140, 3017–3038, <https://doi.org/10.1175/MWR-D-11-00352.1>, 2012.
315
- Gadde, S. N. and Stevens, R. J.: Effect of low-level jet height on wind farm performance, *Journal of Renewable and Sustainable Energy*, 13, <https://doi.org/10.1063/5.0026232>, 2021.
- Haupt, S. E., Kosović, B., Berg, L. K., Kaul, C. M., Churchfield, M., Mirocha, J., Allaerts, D., Brummet, T., Davis, S., DeCastro, A., Dettling, S., Draxl, C., Gagne, D. J., Hawbecker, P., Jha, P., Juliano, T., Lassman, W., Quon, E., Rai, R. K., Robinson, M., Shaw, W., and Thedin, R.:
320 Lessons learned in coupling atmospheric models across scales for onshore and offshore wind energy, *Wind Energy Science*, 8, 1251–1275, <https://doi.org/10.5194/wes-8-1251-2023>, 2023.
- Jungo, G. V., Wu, Y.-T., and Porté-Agel, F.: Field measurements of wind turbine wakes with lidars, *Journal of Atmospheric and Oceanic Technology*, 30, 274–287, <https://doi.org/10.1175/JTECH-D-12-00051.1>, 2013.
- Jensen, N. O.: A note on wind generator interaction, Risø National Laboratory, 1983.
- 325 Jiménez, Á., Crespo, A., and Migoya, E.: Application of a LES technique to characterize the wake deflection of a wind turbine in yaw, *Wind energy*, 13, 559–572, <https://doi.org/10.1002/we.380>, 2010.
- Katic, I., Højstrup, J., and Jensen, N. O.: A Simple Model for Cluster Efficiency, in: EWEC’86. Proceedings, edited by Palz, W. and Sesto, E., vol. 1, pp. 407–410, A. Raguzzi, https://backend.orbit.dtu.dk/ws/files/106427419/A_Simple_Model_for_Cluster_Efficiency_EWEC_86_.pdf, accessed: 2025-12-03, 1987.
- 330 Krishnamurthy, R., Newsom, R. K., Chand, D., and Shaw, W. J.: Boundary layer climatology at ARM Southern Great Plains, Tech. rep., Pacific Northwest National Lab.(PNNL), Richland, WA (United States), <https://doi.org/10.2172/1778833>, 2021.
- Krishnamurthy, R., Newsom, R. K., Kaul, C. M., Letizia, S., Pekour, M., Hamilton, N., Chand, D., Flynn, D., Bodini, N., and Moriarty, P.: Observations of wind farm wake recovery at an operating wind farm, *Wind Energy Science*, 10, 361–380, <https://doi.org/10.5194/wes-10-361-2025>, 2025.
- 335 Larsen, G. C., Aagaard Madsen, H., Bingöl, F., Mann, J., Ott, S., Sørensen, J. N., Okulov, V., Troldborg, N., Nielsen, N. M., Thomsen, K., Larsen, T. J., and Mikkelsen, R.: Dynamic Wake Meandering Modeling, Technical Report Risø-R-1607(EN), Risø National Laboratory, Forskningscenter Risø, Denmark, https://backend.orbit.dtu.dk/ws/portalfiles/portal/7703042/ris_r_1607.pdf, accessed: 2025-12-03, 2007.
- Larsen, T. J., Madsen, H. A., Larsen, G. C., and Hansen, K. S.: Validation of the dynamic wake meander model for loads and power production in the Egmond aan Zee wind farm, *Wind Energy*, 16, 605–624, <https://doi.org/10.1002/we.1563>, 2013.



- 340 Larsén, X. G. and Fischereit, J.: A case study of wind farm effects using two wake parameterizations in the Weather Research and Forecasting (WRF) model (V3. 7.1) in the presence of low-level jets, *Geoscientific Model Development*, 14, 3141–3158, <https://doi.org/10.5194/gmd-14-3141-2021>, 2021.
- Lee, J. C. and Fields, M. J.: An overview of wind energy production prediction bias, losses, and uncertainties, *Wind Energy Science*, 6, 311–365, <https://doi.org/10.5194/wes-6-311-2021>, 2020.
- 345 Letizia, S. and Iungo, G. V.: Pseudo-2D RANS: A LiDAR-driven mid-fidelity model for simulations of wind farm flows, *Journal of Renewable and Sustainable Energy*, 14, 023 301, <https://doi.org/10.1063/5.0076739>, 2022.
- Letizia, S., Bodini, N., Brugger, P., Scholbrock, A., Hamilton, N., Porté-Agel, F., Doubrawa, P., and Moriarty, P.: Holistic scan optimization of nacelle-mounted lidars for inflow and wake characterization at the RAAW and AWAKEN field campaigns, *Journal of Physics: Conference Series*, 2505, 012 048, <https://doi.org/10.1088/1742-6596/2505/1/012048>, 2023.
- 350 Letizia, S., Robey, R., Bodini, N., Sanchez-Gomez, M., Lundquist, J. K., Krishnamurthy, R., and Moriarty, P. J.: Tilted lidar profiling: Development and testing of a novel scanning strategy for inhomogeneous flows, *Journal of Renewable and Sustainable Energy*, 16, 043 310, <https://doi.org/10.1063/5.0209729>, 2024.
- Lissaman, P. B.: Energy effectiveness of arbitrary arrays of wind turbines, *Journal of energy*, 3, 323–328, <https://doi.org/10.2514/3.62441>, 1979.
- 355 Lundquist, J. K., DuVivier, K. K., Kaffine, D., and Tomaszewski, J. M.: Costs and consequences of wind turbine wake effects arising from uncoordinated wind energy development, *Nature Energy*, 4, 26–34, <https://doi.org/10.1038/s41560-018-0281-2>, 2019.
- Magnusson, M. and Smedman, A.-S.: Influence of atmospheric stability on wind turbine wakes, *Wind Engineering*, 18:3, 139–152, 1994.
- Modali, P. K., Vinod, A., and Banerjee, A.: Towards a better understanding of yawed turbine wake for efficient wake steering in tidal arrays, *Renewable Energy*, 177, 482–494, <https://doi.org/10.1016/j.renene.2021.05.152>, 2021.
- 360 Moriarty, P., Abraham, A., Bodini, N., Goldberger, L., Hamilton, N., Hirth, B., Iungo, G. V., Jordan, A. M., Kaul, C. M., Letizia, S., Lundquist, J. K., Moss, C., Pichugina, Y., Radünz, W. C., Vöhringer, A. L., Voss, A., Wise, A. S., Bärfuss, K. B., Barthelmie, R. J., Pryor, S. C., Canadillas, B., Cheung, L., Chow, F. K., Frère, A., Herges, T., Krishnamurthy, R., Klein, P. M., Lampert, A., Puccioni, M., Roy, S., Shams Solari, M., Sanchez-Gomez, M., Scholbrock, A., Shartzter, S., Smith, E. N., Turner, D. D., and Wharton, S.: Wind Farm Atmosphere Interactions as Seen in the American WAKE Experiment (AWAKEN), *Bulletin of the American Meteorological Society*, in review.
- 365 Moriarty, P., Sanz Rodrigo, J., Gancarski, P., Chuchfield, M., Naughton, J. W., Hansen, K. S., Machefaux, E., Maguire, E., Castellani, F., Terzi, L., Breton, S.-P., and Ueda, Y.: IEA-Task 31 WAKEBENCH: Towards a protocol for wind farm flow model evaluation. Part 2: Wind farm wake models, *Journal of Physics: Conference Series*, 524, 012 185, <https://doi.org/10.1088/1742-6596/524/1/012185>, 2014.
- Moriarty, P., Hamilton, N., Debnath, M., Herges, T., Isom, B., Lundquist, J. K., Maniaci, D., Naughton, B., Pauly, R., Roadman, J., Shaw, W., van Dam, J., and Wharton, S.: American WAKE experiment (AWAKEN), Tech. rep., National Renewable Energy Laboratory (NREL), Golden, CO (United States), <https://doi.org/10.2172/1659798>, 2020.
- 370 Moriarty, P., Bodini, N., Letizia, S., Abraham, A., Ashley, T., Bärfuss, K. B., Barthelmie, R. J., Brewer, A., Brugger, P., Feuerle, T., Frère, A., Goldberger, L., Gottschall, J., Hamilton, N., Herges, T., Hirth, B., Hung, L.-Y. L., Iungo, G. V., Ivanov, H., Kaul, C., Kern, S., Klein, P., Krishnamurthy, R., Lampert, A., Lundquist, J. K., Morris, V. R., Newsom, R., Pekour, M., Pichugina, Y., Porté-Agel, F., Pryor, S. C., Scholbrock, A., Schroeder, J., Shartzter, S., Simley, E., Vöhringer, L., Wharton, S., and Zalkind, D.: Overview of preparation for the American WAKE Experiment (AWAKEN), *Journal of Renewable and Sustainable Energy*, 16, <https://doi.org/10.1063/5.0141683>, 2024.
- NREL: ROSCO. Version 2.9, <https://github.com/NREL/ROSCO>, 2021.



- NREL: OpenFast. Version 3.5.2, <https://github.com/OpenFAST/openfast>, 2025a.
- NREL: WISDEM/WEIS, <https://github.com/WISDEM>, 2025b.
- 380 NREL: OpenFAST Turbine Models, <https://github.com/NREL/openfast-turbine-models/tree/main/IEA-scaled>, 2025c.
- Nygaard, N., Poulsen, L., Svensson, E., and Pedersen, J. G.: Large-scale benchmarking of wake models for offshore wind farms, *Journal of Physics: Conference Series*, 2265, 022 008, <https://doi.org/10.1088/1742-6596/2265/2/022008>, 2022.
- Peña, A. and Santos, P.: Lidar observations and numerical simulations of an atmospheric hydraulic jump and mountain waves, *Journal of Geophysical Research: Atmospheres*, 126, e2020JD033 744, <https://doi.org/10.1029/2020JD033744>, 2021.
- 385 Perr-Sauer, J., Optis, M., Fields, J. M., Bodini, N., Lee, J. C., Todd, A., Simley, E., Hammond, R., Phillips, C., Lunacek, M., Kemper, T., Williams, L., Craig, A., Agarwal, N., Sheng, S., and Meissner, J.: OpenOA: An Open-Source Codebase For Operational Analysis of Wind Farms, *Journal of Open Source Software*, 6, 2171, <https://doi.org/10.21105/joss.02171>, 2021.
- Platis, A., Siedersleben, S. K., Bange, J., Lampert, A., Bärfuss, K., Hankers, R., Cañadillas, B., Foreman, R., Schulz-Stellenfleth, J., Djath, B., Neumann, T., and Emeis, S.: First in situ evidence of wakes in the far field behind offshore wind farms, *Scientific reports*, 8, 2163, <https://doi.org/10.1038/s41598-018-20389-y>, 2018.
- 390 Quint, D., Lundquist, J. K., and Rosencrans, D.: Simulations suggest offshore wind farms modify low-level jets, *Wind Energy Science*, 10, 117–142, <https://doi.org/10.5194/wes-10-117-2025>, 2025.
- Radünz, W., Carmo, B., Lundquist, J. K., Letizia, S., Abraham, A., Wise, A. S., Sanchez Gomez, M., Hamilton, N., Rai, R. K., and Peixoto, P. S.: Influence of simple terrain on the spatial variability of a low-level jet and wind farm performance in the AWAKEN field campaign, *Wind Energy Science*, 10, 2365–2393, <https://doi.org/10.5194/wes-10-2365-2025>, 2025.
- 395 Rai, R. K., Kaul, C. M., Chand, D., Goldberger, L. A., Pekour, M., Krishnamurthy, R., Newsom, R. K., Bodini, N., Moriarty, P., and Letizia, S.: Impacts of Wind Farms on the Vertical Structure of Low-Level Jets Based on WRF Simulations and Observations over the AWAKEN Site, submitted to *Wind Energy Science*, 2026.
- Sanz Rodrigo, J., Gancarski, P., Chavez Arroyo, R., Moriarty, P., Chuchfield, M., Naughton, J. W., Hansen, K. S., Macheffaux, E., Koblitz, T., Maguire, E., Castellani, F., Terzi, L., Breton, S.-P., Ueda, Y., Prospathopoulos, J., Oxley, G. S., Peralta, C., Zhang, X., and Witha, B.: IEA-Task 31 WAKEBENCH: Towards a protocol for wind farm flow model evaluation. part 1: Flow-over-terrain models, *Journal of Physics: Conference Series*, 524, 012 105, <https://doi.org/10.1088/1742-6596/524/1/012105>, 2014.
- 400 Skamarock, W. C., Klemp, J. B., Dudhia, J., Gill, D. O., Barker, D. M., Duda, M. G., Huang, X.-Y., Wang, W., and Powers, J. G.: A description of the advanced research WRF version 3, NCAR technical note, 475, 10–5065, https://www2.mmm.ucar.edu/wrf/users/docs/attic/arw_v3_bw.pdf, 2008.
- 405 Stergiannis, N., Lacor, C., Beeck, J., and Donnelly, R.: CFD modelling approaches against single wind turbine wake measurements using RANS, *Journal of Physics: Conference Series*, 753, 032 062, <https://doi.org/10.1088/1742-6596/753/3/032062>, 2016.
- Sun, H., Yang, H., and Gao, X.: Investigation into wind turbine wake effect on complex terrain, *Energy*, 269, 126 767, <https://doi.org/10.1016/j.energy.2023.126767>, 2023.
- 410 Thomsen, K. and Sørensen, P.: Fatigue loads for wind turbines operating in wakes, *Journal of wind engineering and industrial aerodynamics*, 80, 121–136, [https://doi.org/10.1016/S0167-6105\(98\)00194-9](https://doi.org/10.1016/S0167-6105(98)00194-9), 1999.
- Tomaszewski, J. M. and Lundquist, J. K.: Observations and simulations of a wind farm modifying a thunderstorm outflow boundary, *Wind Energy Science*, 6, 1–13, <https://doi.org/10.5194/wes-6-1-2021>, 2021.
- Turner, D. D. and Löhnert, U.: Ground-based temperature and humidity profiling: combining active and passive remote sensors, *Atmospheric Measurement Techniques*, 14, 3033–3048, <https://doi.org/10.5194/amt-14-3033-2021>, 2021.
- 415



- van der Laan, M. P., Kelly, M., Baungaard, M., and Dicholkar, A.: A simple steady-state inflow model of the neutral and stable atmospheric boundary layer applied to wind turbine wake simulations, *Wind Energy Science*, 9, 1985–2000, <https://doi.org/10.5194/wes-9-1985-2024>, 2024.
- Vanderwende, B. J., Kosović, B., Lundquist, J. K., and Mirocha, J. D.: Simulating effects of a wind-turbine array using LES and RANS, *Journal of Advances in Modeling Earth Systems*, 8, 1376–1390, <https://doi.org/10.1002/2016MS000652>, 2016.
- 420 Volker, P. J., Badger, J., Hahmann, A. N., and Ott, S.: The Explicit Wake Parametrisation V1. 0: a wind farm parametrisation in the mesoscale model WRF, *Geoscientific Model Development*, 8, 3715–3731, <https://doi.org/10.5194/gmd-8-3715-2015>, 2015.
- Vollmer, L., Steinfeld, G., Heinemann, D., and Kühn, M.: Estimating the wake deflection downstream of a wind turbine in different atmospheric stabilities: an LES study, *Wind Energy Science*, 1, 129–141, <https://doi.org/10.5194/wes-1-129-2016>, 2016.
- 425 Wildmann, N., Kigle, S., and Gerz, T.: Coplanar lidar measurement of a single wind energy converter wake in distinct atmospheric stability regimes at the Perdigão 2017 experiment, *Journal of Physics: Conference Series*, 1037, 052006, <https://doi.org/10.1088/1742-6596/1037/5/052006>, 2018.
- Wind Data Hub: The American WAKE experimeNt (AWAKEN), <https://doi.org/10.21947/AWAKEN/1914202>, 2022.
- Wise, A. S., Neher, J. M., Arthur, R. S., Mirocha, J. D., Lundquist, J. K., and Chow, F. K.: Meso- to microscale modeling of atmospheric stability effects on wind turbine wake behavior in complex terrain, *Wind Energy Science*, 7, 367–386, <https://doi.org/10.5194/wes-7-367-2022>, 2022.
- 430 Wu, S., Archer, C. L., and Mirocha, J. D.: New insights on wind turbine wakes from large-eddy simulation: Wake contraction, dual nature, and temperature effects, *Wind Energy*, 27, 1130–1151, <https://doi.org/10.1002/we.2827>, 2024.
- Wu, Y.-T. and Porté-Agel, F.: Atmospheric turbulence effects on wind-turbine wakes: An LES study, *energies*, 5, 5340–5362, <https://doi.org/10.3390/en5125340>, 2012.
- 435 Yan, J., Möhrlen, C., Göçmen, T., Kelly, M., Wessel, A., and Giebel, G.: Uncovering wind power forecasting uncertainty sources and their propagation through the whole modelling chain, *Renewable and Sustainable Energy Reviews*, 165, 112519, <https://doi.org/10.1016/j.rser.2022.112519>, 2022.
- Zhou, B. and Chow, F. K.: Nested Large-Eddy Simulations of the Intermittently Turbulent Stable Atmospheric Boundary Layer over Real Terrain, *Journal of the Atmospheric Sciences*, 71, 1021–1039, <https://doi.org/10.1175/JAS-D-13-0168.1>, 2014.
- 440